PHYSICAL REVIEW A **66**, 053618 (2002)

Simulations of thermal Bose fields in the classical limit

M. J. Davis,[1,2,*] S. A. Morgan,[2,3] and K. Burnett[2]

[1]*Department of Physics, University of Queensland, St Lucia, Queensland 4072, Australia*

[2]*Clarendon Laboratory, Department of Physics, University of Oxford, Oxford OX1 3PU, United Kingdom*

[3]*Department of Physics and Astronomy, University College London, Gower Street, London WC1E 6BT, United Kingdom*

(Received 31 January 2002; published 25 November 2002)

We demonstrate that the time-dependent projected Gross-Pitaevskii equation (GPE) derived earlier [M. J. Davis, R. J. Ballagh, and K. Burnett, J. Phys. B **34**, 4487 (2001)] can represent the highly occupied modes of a homogeneous, partially-condensed Bose gas. Contrary to the often held belief that the GPE is valid only at zero temperature, we find that this equation will evolve randomized initial wave functions to a state describing thermal equilibrium. In the case of small interaction strengths or low temperatures, our numerical results can be compared to the predictions of Bogoliubov theory and its perturbative extensions. This demonstrates the validity of the GPE in these limits and allows us to assign a temperature to the simulations unambiguously. However, the GPE method is nonperturbative, and we believe it can be used to describe the thermal properties of a Bose gas even when Bogoliubov theory fails. We suggest a different technique to measure the temperature of our simulations in these circumstances. Using this approach we determine the dependence of the condensate fraction and specific heat on temperature for several interaction strengths, and observe the appearance of vortex networks. Interesting behavior near the critical point is observed and discussed.

DOI: 10.1103/PhysRevA.66.053618 PACS number(s): 03.75.Fi, 05.30.Jp, 11.10.Wx

I. INTRODUCTION

The observation of Bose-Einstein condensation (BEC) in dilute alkali-metal gases [2–4] heralds a new era in the study of quantum fields. It offers a unique opportunity to carry out experiments in the laboratory for which theoretical calculations beginning from a microscopic model of the system are tractable. However, such calculations are fraught with difficulties at finite temperatures. While equilibrium perturbation theories have had much success [5–7] dynamical calculations often require severe approximations to be made.

In Ref. [1] we developed an approximate formalism to describe the dynamics of a thermal Bose condensate based on the Gross-Pitaevskii equation (GPE). This description is valid when the low-lying modes of the system are classical, satisfying the criterion $N_k \gg 1$. This is analogous to the situation in laser physics, where the highly occupied laser modes can be well described by classical equations. We proceeded by dividing the field operator into a classical region represented by a wave function $\psi(\mathbf{x})$ describing the condensate and its coherent excitations, with the remainder of the field described by the quantum operator $\hat{\eta}(\mathbf{x})$. We derived an equation of motion for $\psi(\mathbf{x})$ that we called the finite temperature Gross-Pitaevskii equation (FTGPE).

The FTGPE is a rather complicated equation, however, and in Ref. [8] we briefly described the first results from the simpler projected Gross-Pitaevkskii equation (PGPE) obtained by neglecting the operator $\hat{\eta}(\mathbf{x})$. These results demonstrate that the GPE alone can represent thermal Bose gases. In this paper we elaborate on these results and describe our method in more detail. We also consider the effect of strong particle interactions on the thermal distributions and investigate the appearance of vortices in our simulations.

The use of the dynamical GPE at finite temperature was originally proposed by Svistunov, and co-workers [9–12]. Despite this suggestion first appearing in 1991, there have been relatively few numerical studies based on this approach. Damle *et al.* have performed calculations of the approach to equilibrium of a near ideal superfluid [13], while Marshall *et al.* [14] carried out a qualitative study of evaporative cooling using a two-dimensional (2D) GPE. References [15–20] also use classical methods to represent thermal Bose-condensed systems. Similar approximations to other quantum field equations have been successful elsewhere [21].

This paper is organized as follows. In Sec. II we give a brief derivation of the finite temperature Gross-Pitaevskii equation. In Sec. III we describe and justify the simplification of the FTGPE to the projected Gross-Pitaevskii equation, before describing the simulations we have carried out in Sec. IV. Section V presents the qualitative evidence that the simulations have reached equilibrium, while Sec. VI carries out a quantitative analysis of our numerical data. Section VII discusses the behavior of the condensate fraction, specific heat, and vorticity of the system with temperature, before we conclude in Sec. VIII.

II. OUTLINE OF FORMALISM

A full derivation of the FTGPE and a discussion of the physics described by each of the terms can be found in Ref. [1]. Here we outline the derivation beginning with the equation of motion for the Bose field operator

$$i\hbar \frac{\partial \hat{\Psi}(\mathbf{x})}{\partial t} = \hat{H}_{sp}\hat{\Psi}(\mathbf{x}) + U_0 \hat{\Psi}^{\dagger}(\mathbf{x})\hat{\Psi}(\mathbf{x})\hat{\Psi}(\mathbf{x}), \qquad (1)$$

where $U_0 = 4\pi\hbar^2 a/m$ is the effective interaction strength at

*Electronic address: mdavis@physics.uq.edu.au

low momenta, a is the s-wave scattering length, and m is the particle mass. $\hat{H}_{sp}$ is the single-particle Hamiltonian defined by

$$\hat{H}_{sp} = -\frac{\hbar^2}{2m}\nabla^2 + V_{\text{trap}}(\mathbf{x}), \tag{2}$$

where $V_{\text{trap}}(\mathbf{x})$ is the external trapping potential, if any is present.

The route to the usual GPE is to assume that the full field operator can be replaced by a wave function $\psi(\mathbf{x})$—i.e., that *all* quantum fluctuations can be neglected. We proceed instead by defining a projection operator $\hat{\mathcal{P}}$ such that

$$\hat{\mathcal{P}}\hat{\Psi}(\mathbf{x}) = \sum_{\mathbf{k}\in C} \hat{a}_{\mathbf{k}}\phi_{\mathbf{k}}(\mathbf{x}), \tag{3}$$

where the region C is *determined* by the requirement that $N_{\mathbf{k}} \equiv \langle \hat{a}_{\mathbf{k}}^\dagger \hat{a}_{\mathbf{k}} \rangle \gg 1$, and the set $\{\phi_{\mathbf{k}}\}$ defines some basis in which the Hamiltonian is approximately diagonal at the boundary of C. For these modes, the quantum fluctuation part of the projected field operator can be ignored, and so we replace $\hat{a}_{\mathbf{k}} \to c_{\mathbf{k}}$ and write

$$\psi(\mathbf{x}) = \sum_{\mathbf{k}\in C} c_{\mathbf{k}}\phi_{\mathbf{k}}(\mathbf{x}). \tag{4}$$

Defining the operator $\hat{\mathcal{Q}} = \hat{1} - \hat{\mathcal{P}}$ and $\hat{\mathcal{Q}}\hat{\Psi}(\mathbf{x}) = \hat{\eta}(\mathbf{x})$, operating on Eq. (1) with $\hat{\mathcal{P}}$ and taking the mean value results in what we call the finite temperature GPE,

$$\begin{aligned} i\hbar\frac{\partial\psi(\mathbf{x})}{\partial t} &= \hat{H}_{sp}\psi(\mathbf{x}) + U_0\hat{\mathcal{P}}\{|\psi(\mathbf{x})|^2\psi(\mathbf{x})\} \\ &\quad + U_0\hat{\mathcal{P}}\{2|\psi(\mathbf{x})|^2\langle\hat{\eta}(\mathbf{x})\rangle + \psi(\mathbf{x})^2\langle\hat{\eta}^\dagger(\mathbf{x})\rangle\} \\ &\quad + U_0\hat{\mathcal{P}}\{\psi^*(\mathbf{x})\langle\hat{\eta}(\mathbf{x})\,\hat{\eta}(\mathbf{x})\rangle + 2\psi(\mathbf{x}) \\ &\quad \times\langle\hat{\eta}^\dagger(\mathbf{x})\,\hat{\eta}(\mathbf{x})\rangle\} + U_0\hat{\mathcal{P}}\{\langle\hat{\eta}^\dagger(\mathbf{x})\,\hat{\eta}(\mathbf{x})\,\hat{\eta}(\mathbf{x})\rangle\}. \end{aligned} \tag{5}$$

This equation describes the full dynamics of the coherent region and its coupling to an effective heat bath described by $\hat{\eta}(\mathbf{x})$. In general, the nonequilibrium evolution depends on the coupling between these two regions and the exchange of energy and particles that this allows. The FTGPE must be complemented by an equation of motion for $\hat{\eta}(\mathbf{x})$ and in principle this can be obtained using a form of quantum kinetic theory.

The only approximation that has been made in the derivation of the FTGPE is that the modes represented by $\psi(\mathbf{x})$ must satisfy the criterion of classicality, that is $N_k \gg 1$. The FTGPE is a nonperturbative equation, and therefore we expect that it will be valid in the region of the phase transition, as long as only the highly occupied modes are treated. There is perhaps a misperception in the BEC community that the GPE is only valid at $T=0$. However, it is well known that close to the phase transition a classical description of the long length scales involved is completely appropriate. This is exactly what the GPE describes, and in fact it has been used as a model of phase transitions in other areas of condensed matter physics. Indeed our model has the same energy functional for these modes as used in the classical renormalization group theory of the superfluid phase transition. It therefore seems reasonable to expect that the same approximations are valid in this case.

The physical processes described by the various terms of Eq. (5) are discussed in detail in Ref. [1]. In this paper, we concentrate on a simplification of the FTGPE which is effectively a model of a restricted system. This allows us to demonstrate some of the properties of the GPE without having to solve the more complicated equation.

III. THE PROJECTED GPE

In this paper, we wish to show that the GPE *alone* can describe evolution of general configurations of the coherent region C towards an equilibrium that can be parametrized by a temperature. We therefore ignore all terms involving $\hat{\eta}(\mathbf{x})$ in Eq. (5) and concentrate on the first line,

$$i\hbar\frac{\partial\psi(\mathbf{x})}{\partial t} = \hat{H}_{sp}\psi(\mathbf{x}) + U_0\hat{\mathcal{P}}\{|\psi(\mathbf{x})|^2\psi(\mathbf{x})\}, \tag{6}$$

which we call the projected GPE. Although Eq. (6) is completely reversible, it is well known that deterministic nonlinear systems with only a few degrees of freedom exhibit chaotic, and hence ergodic behavior [22]. If many modes are occupied, the projected GPE contains many degrees of freedom and it is therefore reasonable to expect it to evolve to equilibrium (except for specially chosen initial conditions such as eigenstate solutions).

The projected GPE describes a microcanonical system. However, if the region C is large, then its fluctuations in energy and particle number in the grand canonical ensemble would be small. Hence we expect the final equilibrium state of the projected GPE to be similar to that of the finite temperature GPE coupled to a bath $\hat{\eta}(\mathbf{x})$ with the appropriate chemical potential and temperature. The detailed nonequilibrium dynamics of the system *will* depend on the exchange of energy and particles between C and the bath—however, we leave the coupling of $\psi(\mathbf{x})$ and $\hat{\eta}(\mathbf{x})$ to be addressed in future work.

A. The projector

The spatial representation of the projection operation is written as

$$\hat{\mathcal{P}}\{F(\mathbf{x})\} = \sum_{k\in C}\phi_k(\mathbf{x})\int d^3\mathbf{x}'\,\phi_k^*(\mathbf{x}')F(\mathbf{x}'), \tag{7}$$

and this operation must be carried out numerically every time we calculate the nonlinear term in the PGPE. This is a very time consuming operation in general, taking many times longer than calculating $|\psi(\mathbf{x})|^2\psi(\mathbf{x})$ itself.

The operation is much simpler numerically if we use a plane-wave basis in our projector

$$\phi_k(\mathbf{x}) = \frac{\exp(i\mathbf{k}\cdot\mathbf{x})}{\sqrt{V}}, \tag{8}$$

where V is the volume of our system. In this case Eq. (7) becomes simply the application of a forward Fourier transform to our function $F(\mathbf{x})$, followed by an inverse Fourier transformation that includes only the modes in the coherent region. Thus our numerical procedure is

$$\hat{\mathcal{P}}\{F(\mathbf{x})\} = \mathcal{O}_{\mathrm{IFFT}}\{P(\mathbf{k})\mathcal{O}_{\mathrm{FFT}}[F(\mathbf{x})]\}, \tag{9}$$

where $\mathcal{O}_{\mathrm{FFT}}$ and $\mathcal{O}_{\mathrm{IFFT}}$ refer to the forward and inverse fast Fourier transform operations respectively, and $P(\mathbf{k})$ is the representation of the projector $\hat{\mathcal{P}}$ in Fourier space. There are very efficient routines available to carry out FFTs, and so we find that it is extremely advantageous numerically to define our projector in the plane-wave basis.

B. Implications

For any nonperiodic trapping potential, the use of a plane-wave basis is at odds with our requirement that the basis must approximately diagonalize the Hamiltonian at the boundary of the region C. In fact, it may not even satisfy this requirement for a periodic potential if the boundary of the coherent region occurs at a low enough energy.

If we consider a homogeneous system, however, the plane-wave basis will always satisfy our requirements. In this case the effect of a condensate on the excitations of the system is simply to mix modes of momenta $\mathbf{p}$ and $-\mathbf{p}$. Thus even if the Hamiltonian is not diagonalized at the boundary of C, we can still apply the projector cleanly in Fourier space. For these reasons, the simulations that we present in this paper are for the homogeneous Bose gas. We intend to address the issue of projectors for the trapped Bose gas in future work.

A direct advantage of simulating the homogeneous system is that the condensate occupation is readily identified as the $\mathbf{k}=0$ component of the wave function. This is in contrast to the trapped case, where the condensate mode changes with the condensate fraction. In general the condensate fraction must be determined by diagonalization, which can be a very time consuming procedure [19].

IV. SIMULATIONS

We have performed simulations for a fully three-dimensional homogeneous Bose gas with periodic boundary conditions. The dimensionless equation we compute is

$$i\frac{\partial\psi(\tilde{\mathbf{x}})}{\partial\tau} = -\tilde{\nabla}^2\psi(\tilde{\mathbf{x}}) + C_{\mathrm{nl}}\hat{\mathcal{P}}\{|\psi(\tilde{\mathbf{x}})|^2\psi(\tilde{\mathbf{x}})\}, \tag{10}$$

where the normalization of the wave function has been defined to be

$$\int d^3\tilde{\mathbf{x}}|\psi(\tilde{\mathbf{x}})|^2 = 1. \tag{11}$$

The nonlinear constant is

$$C_{\mathrm{nl}} = \frac{2mNU_0}{\hbar^2 L}, \tag{12}$$

where N is the total number of particles in the system, and L is the period. Our dimensionless parameters are $\tilde{\mathbf{x}}=\mathbf{x}/L$, wave vector $\tilde{\mathbf{k}}=\mathbf{k}L$, energy $\tilde{\varepsilon}=\varepsilon/\varepsilon_L$, and time $\tau=\varepsilon_L t/\hbar$, with $\varepsilon_L=\hbar^2/(2mL^2)$.

A. Parameters

The two parameters that determine all properties of the system are the projector $\hat{\mathcal{P}}$ and the nonlinear constant C_{nl}.

1. Projector $\hat{\mathcal{P}}$

We have chosen a projection operator such that all modes included in the simulations have $|\mathbf{k}|<15\times 2\pi/L$, which enables us to use a computationally efficient numerical grid of $32\times 32\times 32$ points. This means that 13 997 modes are included in the system.

Grid size and aliasing. The nonlinear term of the GPE can generate momentum components up to three times larger than those which exist in the original wave function. Thus it would seem that calculating the term $|\psi(\mathbf{x})|^2\psi(\mathbf{x})$ on a grid only slightly larger than the projector would cause problems with aliasing. The correct procedure would be instead to calculate this term on a grid size of $96\times 96\times 96$ points before performing the projection operation.

To check the effect of grid size we have performed simulations where the nonlinear term was calculated on grids of size 32, 64, and 96 points, and found that there is no difference in the equilibrium properties of the system. The detailed dependence of the condensate population during evolution is different in detail for each size grid, but follows the same average curve. The same behavior is observed when adjusting the accuracy parameter of our adaptive step size algorithm for evolving the GPE.

We attribute this behavior to the deterministic chaos exhibited by the system. Any small numerical error is eventually magnified such that the system follows a quite different microscopic path through phase space, although the resulting macroscopic (average) properties are unaffected.

2. Nonlinearity C_{nl}

We note that the choice of the nonlinear constant determines only the ratio of NU_0/L. This means that for a given value of C_{nl}, we can choose the parameters N, U_0, and L such that our condition $N_{\mathbf{k}}\equiv N|c_{\mathbf{k}}|^2 \gg 1$ is always satisfied for a given physical situation.

We have performed three series of simulations with nonlinearities of $C_{\mathrm{nl}}=500$, 2000, and 10 000. The highest value of C_{nl} was chosen such that all the states contained in the calculation are phononlike for a large condensate fraction.

The boundary between phononlike and particlelike states for the homogeneous gas is

$$\frac{\hbar^2 k_0^2}{2m} = n_0 U_0, \tag{13}$$

where we have defined N_0 to be the condensate number within the volume L^3, and thus $n_0 = N_0/L^3$ is the condensate density. Converting Eq. (13) to dimensionless units we find that

$$\tilde{k}_0 = \sqrt{C_{\rm nl}\frac{N_0}{N}}, \tag{14}$$

and therefore for a condensate fraction of $N_0/N = 1$ we have

$$C_{\rm nl} = 10\,000 \rightarrow \tilde{k}_0 \approx 15.9 \times 2\pi,$$

$$C_{\rm nl} = 2000 \rightarrow \tilde{k}_0 \approx 7.12 \times 2\pi,$$

$$C_{\rm nl} = 500 \rightarrow \tilde{k}_0 \approx 3.56 \times 2\pi.$$

We find that computations with smaller values of $C_{\rm nl}$ take comparatively longer to reach equilibrium. This is because the equilibration rate is approximately proportional to $C_{\rm nl}^2$, whereas the minimum time step allowed for a given accuracy in the numerical integration of the PGPE only increases slowly with decreasing $C_{\rm nl}$.

To give an indication of how these dimensionless parameters compare to experimental setups, for $C_{\rm nl} = 10\,000$ we can choose ^{87}Rb atoms with $N = 1.8 \times 10^6$ and $L \approx 26$ μm to give a number density of about 10^{14} cm^{-3}—similar to current experiments on BEC in traps.

B. Initial wave functions

We begin our simulations with strongly nonequilibrium wave functions with a chosen total energy $\tilde{E}$. We construct these by populating the amplitudes of the wave function components $c_{\mathbf{k}}$ in the expansion

$$\psi(\mathbf{x},0) = \sum_{\mathbf{k}\in C} c_{\mathbf{k}} e^{i\mathbf{k}\cdot\mathbf{x}}. \tag{15}$$

The populations $|c_{\mathbf{k}}|^2$ are chosen such that the distribution is as flat as possible, while the phases of the amplitudes are chosen at random [12].

The total energy $\tilde{E}$ is a constraint on the distribution of amplitudes. The energy of a pure condensate is $\tilde{E}_0 = C_{\rm nl}/2$, all of this being due to interactions—the kinetic energy is zero. To have a wave function with an energy not much larger than $C_{\rm nl}/2$, the occupations of the $\tilde{k} = 0$ state and the $\tilde{k} = 2\pi$ states cannot be equal. (We use the notation $\tilde{k} \equiv |\tilde{\mathbf{k}}|$.) Therefore, for the lowest energy simulations the initial condensate population is necessarily larger than the excited state populations.

To ensure that the initial wave functions are sufficiently randomized, we enforce the condition that all 123 states with $\tilde{k} \leqslant 3 \times 2\pi$ must have some initial population, while all other components may be unoccupied. For low energies, when this distribution including the condensate cannot be totally flat, we keep the populations of the components with $1 \leqslant \tilde{k}/2\pi \leqslant 3$ equal, and adjust the condensate population such that the wave function has the energy we require. An example of this situation is shown in Fig. 1(a) for the $\tilde{E} = 7000$ initial wave function in the $C_{\rm nl} = 10\,000$ simulation series.

For simulations with a sufficiently high total energy $\tilde{E}$ that the inner 123 components may have equal population, we continue to add further shells of higher k to our wave function. The amplitudes of the inner components are readjusted to maintain the required normalization. This causes the energy of the system to increase monotonically with each new shell until we find two wave functions that bound the energy we are looking for, differing only in their outermost shell. We then adjust the population of the outermost shell downwards until we reach the required energy.

This procedure is necessary due to the nonlinearity of the problem. In the case of the ideal gas ($C_{\rm nl} = 0$), we can calculate the kinetic energy (and hence the total energy) of the wave function simply by knowing the distribution of $|c_{\mathbf{k}}|^2$, via

$$E_{\rm kin} = -\frac{\hbar^2}{2m}\int d^3\mathbf{x}\, \psi^*(\mathbf{x})\nabla^2\psi(\mathbf{x}),$$

$$= \frac{\hbar^2}{2m}\sum_{\mathbf{k}} |c_{\mathbf{k}}|^2 k^2. \tag{16}$$

However, for $C_{\rm nl} > 0$ we must also add the interaction energy of the wave function to the total energy. This is,

$$E_{\rm int} = \frac{U_0}{2}\int d^3\mathbf{x} |\psi(\mathbf{x})|^4 = \frac{U_0}{2}\sum_{\mathbf{pqmn}} c_{\mathbf{p}}^* c_{\mathbf{q}}^* c_{\mathbf{m}} c_{\mathbf{n}} \delta_{\mathbf{p}+\mathbf{q}-\mathbf{m}-\mathbf{n}}, \tag{17}$$

and depends nontrivially on the $\{c_{\mathbf{k}}\}$.

Further images of initial- and final-state wave functions are shown in Fig. 1 in k space, and Fig. 2 in real space.

C. Evolution

The PGPE is evolved in the interaction picture, using a fourth-order Runge-Kutta method with adaptive step size determined by estimating the fifth-order truncation error. The acceptable relative truncation error was set to be 10^{-10} for all components with an occupation of $\geqslant 10^{-4} N_0/N$. This resulted in typical time steps as presented in Table I, which could be integrated in a reasonable time on a modern workstation.

We evolve the simulations for at least twice as long as it takes for the system to reach equilibrium, based on the observation of the behavior of the condensate fraction (see Sec. V). The time period for each value of $C_{\rm nl}$ is also given in Table I. Thus the longest of these simulations required $\sim 5 \times 10^5$ time steps.

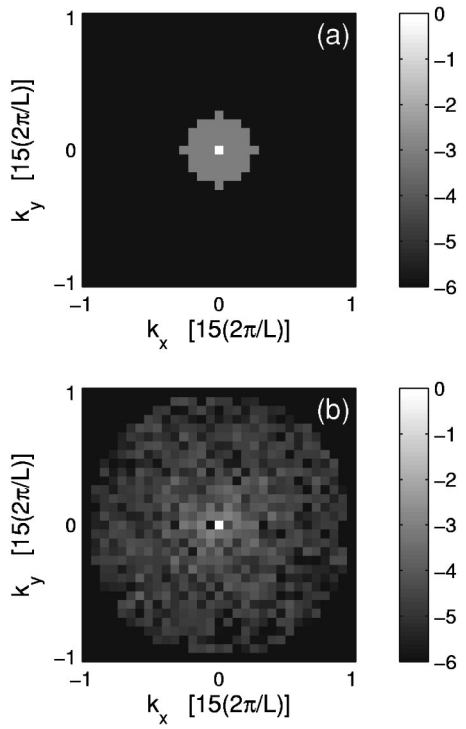

FIG. 1. Two-dimensional slices of wave functions through the $k_z=0$ plane in momentum space for the $C_{\rm nl}=10\,000$, $\tilde{E}=7000$ simulations. (a) Base 10 logarithm of the k-space wave function at $\tau=0$. (b) Base 10 logarithm of the k-space wave function at $\tau=0.2$ once the system has reached equilibrium.

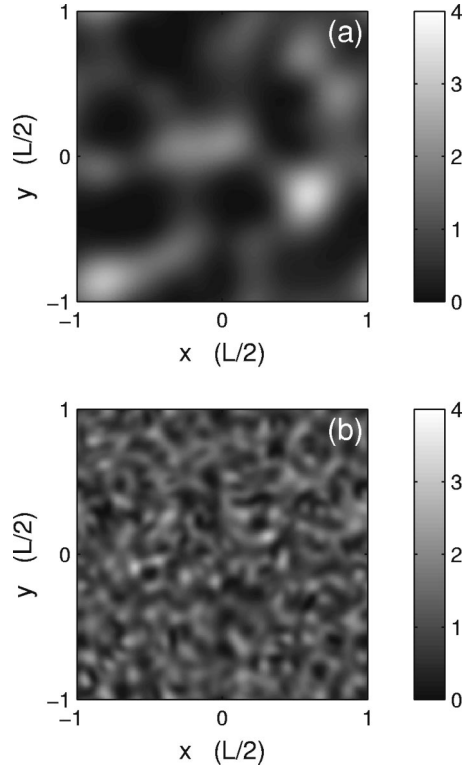

FIG. 2. Two-dimensional slices of wave functions near the $z=0$ plane in real space for the $C_{\rm nl}=10\,000$, $\tilde{E}=7000$ simulations. (a) Base 10 logarithm of the real-space wave function at $\tau=0$. (b) Base 10 logarithm of the real-space wave function at $\tau=0.2$ once the system has reached equilibrium.

V. EVIDENCE FOR EQUILIBRIUM

Although the PGPE is completely reversible, the final-state wave functions displayed in Figs. 1 and 2 indicate that the simulations have evolved the system to an apparent equilibrium state. The k-space distributions have evolved from initially being flat to a form that is peaked at the center, and tails away towards the edges. Also, there is a smoothing out of both the phase and density profiles of the real-space wave function. After a certain time of evolution $\tau_{\rm eq}$, the plots for the wave functions appear to be isomorphic for $\tau>\tau_{\rm eq}$.

We would like to note that the equilibrium properties depend only on the total energy and momentum of the initial wave function—they are independent of the shape of the initial distribution in k space. We have performed simulations with nonspherical initial wave functions, and found that they evolve to a spherical equilibrium state. Also, as the GPE conserves momentum, for the condensate to form in the $k=0$ mode the initial distribution must have zero total momentum. We have performed simulations where the initial distribution had a finite momentum, and observed the condensate to form in a nonzero momentum state as expected.

To determine the properties of the system at equilibrium, in theory we should carry out many different simulations each with the same initial populations but with different choices of the initial phases, and then take the ensemble average. However, this is an extremely large computational task. Instead, we assume the ergodic theorem applies, such that the time average over the evolution of a single system at equilibrium is equivalent to the ensemble average over many different systems. We therefore perform a time-average over the last 50 wave functions saved, all with $\tau>\tau_{\rm eq}$.

A. Condensate occupation

Strong evidence that the simulations have reached equilibrium is provided by the time dependence of the condensate population. For all simulations this settles down to an average value (dependent on the energy $\tilde{E}$) that fluctuates by a small amount. The initial time evolution of the condensate fraction for five different energies with $C_{\rm nl}=10\,000$ is shown in Fig. 3.

The average condensate occupation in equilibrium for all simulations for the $C_{\rm nl}=10\,000$ case are presented in Fig.

TABLE I. The typical minimum and maximum time steps for the simulations. The minimum is for high-energy simulations, and the maximum is for low-energy simulations.

$C_{\rm nl}$	Minimum time step (units of 10^{-6})	Maximum time step (units of 10^{-6})	Length of evolution τ
500	4	6	2.0
2000	1.6	4.4	0.4
10000	0.45	1.2	0.2

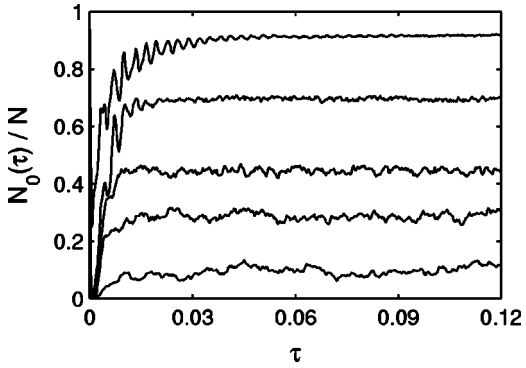

FIG. 3. Plot of the initial time evolution of $N_0(\tau)/N$ for four different simulation energies with $C_{\rm nl}=10\,000$. From top to bottom: $\tilde{E}=5500,7000,8500,9250,10\,000$. The simulations were run until $\tau=0.2$. Other values of the nonlinearity give qualitatively similar results.

4(a). The fluctuations of the condensate population are indicated by the (barely visible) vertical lines at each point, and these are largest for the $\tilde{E}=9000$ simulation. For comparison, the corresponding curve for the ideal gas is plotted in Fig. 4(b). We can see that for $C_{\rm nl}=0$ the curve is linear up to the transition point, but the $C_{\rm nl}=10\,000$ curve displays a

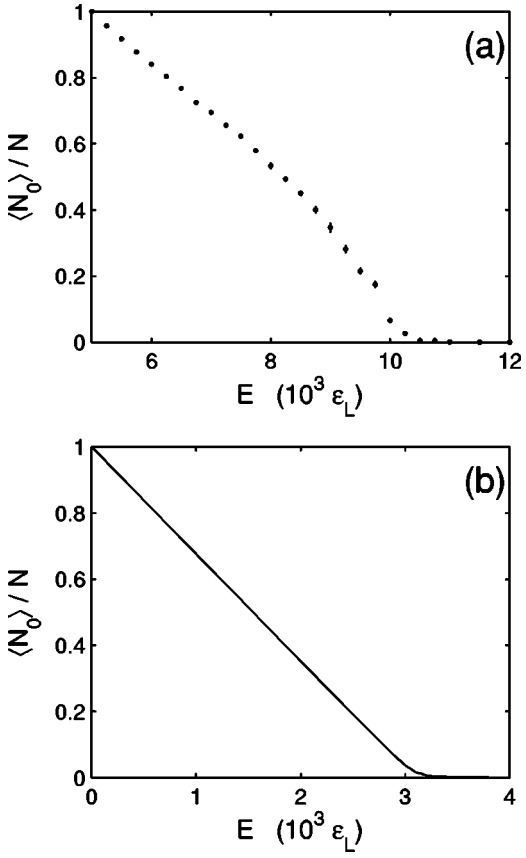

FIG. 4. (a) Condensate fraction plotted against total energy after each individual simulation has reached equilibrium for $C_{\rm nl}=10\,000$. The barely discernible vertical lines on each point indicate the magnitude of the fluctuations. (b) The curve for the same system, but calculated for the ideal gas.

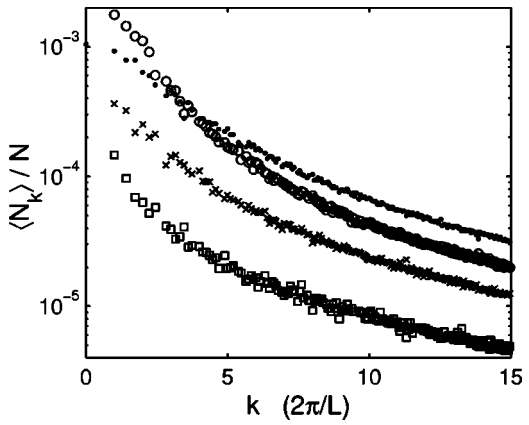

FIG. 5. Plots of the equilibrium Bogoliubov quasiparticle distributions averaged over time and angle for four different total energies. Squares, $\tilde{E}=6000$; crosses, $\tilde{E}=7500$; circles, $\tilde{E}=9000$; dots, $\tilde{E}=11\,000$. The mean condensate occupation for the first three distributions is off axis.

distinct bulge in this region. The shape of the corresponding curves for $C_{\rm nl}=500$ and 2000 fall in between the $C_{\rm nl}=0$ and 10 000 cases.

B. Particle distribution

Further evidence of equilibrium is provided by the distribution of the particles in momentum space. Rather than using the plane-wave basis, we transform the wave functions into the quasiparticle basis of quadratic Bogoliubov theory. For the homogeneous gas, this theory can be solved analytically and we can write the quasiparticle amplitude $b_{\mathbf{k}}$ as

$$b_{\mathbf{k}}=u_{\mathbf{k}}c_{\mathbf{k}}-v_{\mathbf{k}}c_{-\mathbf{k}}, \tag{18}$$

where

$$u_{\mathbf{k}}=\frac{1}{\sqrt{1-\alpha_k^2}}, \quad v_{\mathbf{k}}=\frac{-\alpha_k}{\sqrt{1-\alpha_k^2}}, \tag{19}$$

and α_k is given by

$$\alpha_k=1+y_k^2-y_k\sqrt{2+y_k^2}. \tag{20}$$

In this last equation, the dimensionless wave vector y_k is given by $y_k=k/k_0$ with k_0 as defined in Eq. (13). The normalization condition $u_{\mathbf{k}}^2-v_{\mathbf{k}}^2=1$ is automatically satisfied by Eq. (19). From Eq. (14) we can see that the sole parameters of the transformation are the condensate fraction $\langle N_0\rangle/N$, and the nonlinear constant $C_{\rm nl}$.

We time average the populations of the quasiparticles states $N_{\mathbf{k}}/N=|b_{\mathbf{k}}|^2$ as was described above to give $\langle N_{\mathbf{k}}\rangle/N$, and finally average over angle so that we can produce a one-dimensional plot of $\langle N_k\rangle/N$. This distribution for four different simulation energies and $C_{\rm nl}=10\,000$ is shown in Fig. 5.

We can see that the shape of the curves is surprisingly smooth for each energy, suggesting that the system is in

equilibrium. The plot of the distribution for any individual wave function is scattered about the average.

We have also determined the fluctuations of the population of the quasiparticle modes. The grand canonical ensemble for the Bose gas predicts the relationship

$$\langle \Delta N_k \rangle^2 = \langle N_k \rangle^2 + \langle N_k \rangle \tag{21}$$

for $k \neq 0$, which in the classical limit $\langle N_k \rangle \gg 1$ gives

$$\langle \Delta N_k \rangle \approx \langle N_k \rangle. \tag{22}$$

This is indeed the behavior that we observe. Although we are evolving a microcanonical system, in this case there are such a large number of modes that the remainder of the system acts as a bath for any individual mode and the result still applies.

VI. QUANTITATIVE ANALYSIS OF THE DISTRIBUTIONS

While the data presented in Sec. V indicates that the PGPE is evolving the system to equilibrium, as yet we have presented no quantitative evidence. To demonstrate conclusively that equilibrium has been reached, we need to be able to assign a *temperature* to the simulations. In this section we measure a temperature for a given simulation by comparing the distribution function of the numerical simulations against a predicted energy spectrum.

A. Expected equilibrium distribution

The GPE is the high occupation (classical) limit of the full equation for the Bose field operator, Eq. (1). Therefore, in equilibrium we expect the mean occupation of mode k to be the classical limit of the Bose-Einstein distribution—i.e., the equipartition relation

$$\langle N_k \rangle = \frac{k_B T}{\varepsilon_k - \mu}, \tag{23}$$

where k labels the *eigenstates* of the system. In general these will be some type of quasiparticle mode. Manipulating Eq. (23), we find that

$$\varepsilon_k = \frac{k_B T}{\langle N_k \rangle} + \mu. \tag{24}$$

The equilibrium condensate occupation according to the equipartition relation will be given by Eq. (23) with $\langle N_k \rangle \rightarrow \langle N_0 \rangle$ and $\varepsilon_k \rightarrow \lambda$ (the condensate eigenvalue). From this expression we can solve for the chemical potential

$$\mu = \lambda - \frac{k_B T}{\langle N_0 \rangle}. \tag{25}$$

Substituting this result into Eq. (24), and converting to dimensionless units we find

$$\frac{\tilde{\varepsilon}_k - \tilde{\lambda}}{\tilde{T}} = \left(\frac{N}{\langle N_k \rangle} - \frac{N}{\langle N_0 \rangle} \right), \tag{26}$$

where $\tilde{T} = k_B T/(N\varepsilon_L)$ is the dimensionless temperature.

Once equilibrium has been reached for a single simulation, we make use of Eq. (26) to measure the quantity $\tilde{T}$. Decomposing the wave functions in some basis and time-averaging the populations determines $\langle N_k \rangle / N$ as a function of the variable k, as is plotted in Fig. 5. This completely specifies the RHS of Eq. (26) and it remains to determine the quantities on the LHS.

In this section we consider three different methods of either predicting or measuring the function $\tilde{\varepsilon}_k - \tilde{\lambda}$. If the basis we have used for our decomposition is a good one, and our prediction for $\tilde{\varepsilon}_k - \tilde{\lambda}$ is correct, then this curve will have the same shape as the RHS of Eq. (26). The constant of proportionally determined by a fitting procedure will then give the temperature $\tilde{T}$.

Before we describe our methods and results, we would like to note that the quantity we refer to, throughout the remainder of this paper, as the temperature is the variable $\tilde{T}$ as determined by the numerical fitting procedures described above. We have not yet established that this is the true temperature as defined by thermal equilibrium with a heat reservoir. However, we believe that if we were to solve the FTGPE with $\hat{\eta}(\mathbf{x})$ acting as a heat bath, then the temperature determined in the coherent region via this method would agree with the bath temperature.

B. Method 1: Bogoliubov theory

In the limit of large condensate fraction $\langle N_0 \rangle / N \sim 1$, we expect the Bogoliubov transformation to provide a good basis. For the homogeneous case the dispersion relation is known analytically, and is given by

$$\varepsilon_k - \lambda = \left[\left(\frac{\hbar^2 k^2}{2m} \right)^2 + (c\hbar k)^2 \right]^{1/2}, \tag{27}$$

where $c = (n_0 U_0 / m)^{1/2}$ is the speed of sound and ε_k is the absolute energy of a mode with wave vector k. In our dimensionless units this becomes

$$\tilde{\varepsilon}_k - \tilde{\lambda} = \left(\tilde{k}^4 + 2C_{\mathrm{nl}} \frac{\langle N_0 \rangle}{N} \tilde{k}^2 \right)^{1/2}. \tag{28}$$

The condensate fraction is determined from the numerical results, and so when the Bogoliubov dispersion relation is valid, we can determine a temperature for the simulations by substituting Eq. (28) in Eq. (26).

Results. We have carried out this analysis for all the simulation data. For the $C_{\mathrm{nl}} = 500$ case, the measured distributions are in excellent agreement with the Bogoliubov dispersion relation for all energies, and we have been able to extract the corresponding temperature for each simulation.

However, this is not the case for the more strongly interacting systems. For $C_{\mathrm{nl}} = 2000$, the Bogoliubov relation is a good fit only for simulations with $\tilde{E} \leqslant 2000$ ($\langle N_0 \rangle / N \geqslant 0.75$), or for energies above the BEC transition point. For the $C_{\mathrm{nl}} = 10\,000$ case, good agreement is found only for the lowest energy simulation with $\tilde{E} = 5250$ and $\langle N_0 \rangle / N \approx 0.96$.

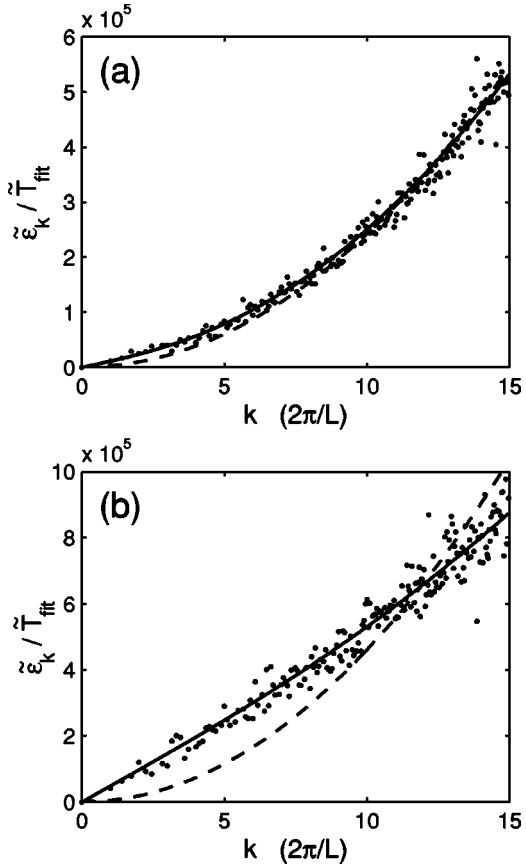

FIG. 6. Fits of the simulation quasiparticle population data to the Bogoliubov dispersion relation for two cases. For both graphs the solid line is the Bogoliubov curve, while the dashed line is the ideal gas dispersion relation. The temperature is determined by a least-squares fit to the plot of $(N/\langle N_k\rangle - N/\langle N_0\rangle)$, which is shown as the dots. (a) $C_{\rm nl}=500$, $\tilde{E}=500$, and $\langle N_0\rangle/N=0.929$, with a best-fit temperature from Bogoliubov theory of $\tilde{T}=0.0175$. (b) $C_{\rm nl}=10\,000$, $\tilde{E}=5250$, and $\langle N_0\rangle/N=0.957$, with a best-fit temperature from Bogoliubov theory of $\tilde{T}=0.018$.

Sample fits of the simulation data to the Bogoliubov dispersion relation are shown in Fig. 6 for cases where the agreement is good. (An example of this procedure where the Bogoliubov spectrum is not appropriate is given in Fig. 8.)

The reason for the limited range of agreement is because the Bogoliubov transformation diagonalizes only a quadratic approximation to the full Hamiltonian. It neglects terms that are cubic and quartic in noncondensate operators, assuming that they are small (these are discussed in detail below). This is a good approximation for the $C_{\rm nl}=500$ simulations—at large condensate fraction the dispersion relation is only slightly shifted from the noninteracting relation $\tilde{\varepsilon}_k=\tilde{k}^2$, and at smaller condensate fractions the difference is negligible. Hence we can fit a temperature up to and above the BEC transition.

For the $C_{\rm nl}=2000$ case the higher-order terms become important above $\tilde{E}=2000$, and for the strongest interaction strength of $C_{\rm nl}=10\,000$, they are important for all but the lowest energy simulation we consider. For the higher-energy simulations the shape of Eq. (26) no longer agrees with Eq. (28), and we must use a more sophisticated theory to predict the dispersion relation.

Above the transition point, however, there is no condensate and the ideal gas dispersion relation is a reasonable description of the system.

C. Method 2: Second-order theory

As the occupation of the quasiparticle modes becomes significant at large interaction strengths, the cubic and quartic terms of the many-body Hamiltonian that are neglected in the Bogoliubov transformation become important. In Ref. [5] Morgan develops a consistent extension of the Bogoliubov theory to second order that leads to a gapless excitation spectrum. This theory treats the cubic and quartic terms of the Hamiltonian using perturbation theory in the Bogoliubov quasiparticle basis. This results in energy shifts of the excitations away from the Bogoliubov predictions of Eq. (27).

Expressions for the energy shifts of the excitations are given in Sec. VI 2 of Ref. [5]. They have the form

$$\Delta\tilde{\varepsilon}_k=\Delta\tilde{E}_3(k)+\Delta\tilde{E}_4(k)+\Delta\tilde{E}_\lambda(k), \tag{29}$$

where $\Delta\tilde{E}_3(k)[\Delta\tilde{E}_4(k)]$ is the shift in energy of a quasiparticle in mode k due to the cubic (quartic) Hamiltonian, and $\Delta\tilde{E}_\lambda(k)$ describes the shift due to the change in the condensate eigenvalue. In the high-occupation limit we find

$$\Delta\tilde{E}_4(k)+\Delta\tilde{E}_\lambda(k)=-C_{\rm nl}\tilde{\kappa}\frac{(1+\alpha_k)^2}{1-\alpha_k^2}, \tag{30}$$

where $\tilde{\kappa}$ is the dimensionless anomalous average, defined by

$$\tilde{\kappa}=\sum_k \frac{(N_k+N_{-k})\alpha_k}{N(1-\alpha_k^2)}. \tag{31}$$

The expression for $\Delta\tilde{E}_3(k)$ is derived from second-order perturbation theory, and is rather complicated. We have

$$\Delta\tilde{E}_3(k)=\frac{-2C_{\rm nl}}{1-\alpha_k^2}[\Delta\tilde{E}_3^a(k)+\Delta\tilde{E}_3^b(k)+\Delta\tilde{E}_3^c(k)], \tag{32}$$

where

$$\Delta\tilde{E}_3^a(k)=\sum_j \frac{(N_i+N_j)(1-\alpha_i-\alpha_j+\alpha_i\alpha_k+\alpha_j\alpha_k-\alpha_i\alpha_j\alpha_k)^2}{N(z_i+z_j-z_k)(1-\alpha_i)^2(1-\alpha_j)^2}, \tag{33}$$

$$\Delta\tilde{E}_3^b(k)=\sum_j \frac{(N_{-i}+N_{-j})(\alpha_i+\alpha_j+\alpha_k-\alpha_i\alpha_j-\alpha_i\alpha_k-\alpha_j\alpha_k)^2}{N(z_i+z_j+z_k)(1-\alpha_i)^2(1-\alpha_j)^2}, \tag{34}$$

$$\Delta\tilde{E}_3^c(k)=\sum_j \frac{(N_i-N_j)(1-\alpha_j-\alpha_k+\alpha_i\alpha_j+\alpha_i\alpha_k-\alpha_i\alpha_j\alpha_k)^2}{N(z_i-z_j+z_k)(1-\alpha_i)^2(1-\alpha_j)^2}, \tag{35}$$

in which $\mathbf{i}=\mathbf{k}-\mathbf{j}$ and

$$z_k=y_k(2+y_k^2)^{1/2}\equiv\tilde{\varepsilon}_k\left(C_{\rm nl}\frac{\langle N_0\rangle}{N}\right)^{-1}, \tag{36}$$

is another form of the dimensionless energy of mode k, with $y_k=k/k_0$ as earlier.

1. Calculation of energy shifts

The numerical calculation of the energy shifts is not a trivial task, and we have used two methods to determine the shifts for our simulations. The first procedure is to calculate the shifts directly using the population data from the simulations. We therefore,

(1) Calculate the quasiparticle populations $N_{\mathbf{k}}$ for the last 50 wave functions of our simulation based on a condensate population $\langle N_0\rangle$, and then average these over time.

(2) Calculate the energy shifts for mode $\mathbf{k}$ using these populations as the input.

(3) Average the shifts over angle to give a one-dimensional function of k.

This results in plots of the energy shifts that are somewhat scattered due to the finite size of the system. The expressions for the shifts Eqs. (33)–(35) contain poles when energy matches occur, and hence the numerical calculation is performed using an imaginary part in the denominator. The size of this imaginary part does not affect the shape of the curve in the limit that it is small, but it does affect the amount of scatter in the shifts. We have performed sample calculations allowing L to increase while keeping other parameters of the system constant, and this makes the curve smoother.

The second procedure only makes use of the condensate fraction and the *total* number of quasiparticles, rather than the population of the individual levels. By assuming the Bogoliubov spectrum is a good estimate of the energies (which must be true for the perturbation theory to be valid), we can estimate the temperature $\tilde{T}_{\rm est}$ using the normalization constraint on the populations

$$\sum_k \frac{\langle N_k\rangle}{N}=\frac{\langle N_0\rangle}{N}+\sum_{k>0}\frac{\tilde{T}_{\rm est}}{\tilde{\varepsilon}_k-\tilde{\lambda}}, \tag{37}$$

where we have used the approximation $\tilde{\mu}=\tilde{\lambda}$ that is valid when there is a condensate present. The LHS as well as the value of $\langle N_0\rangle/N$ are determined by the simulations, and the Bogoliubov relation Eq. (28) is used for the energies.

Once the estimated temperature $T_{\rm est}$ is determined, we use the equipartition Bogoliubov relation for the populations in Eqs. (33)–(35), and then approximate the sums by numerical integration to calculate the shifts to the levels. We find that this gives curves that agree on average with those calculated using the first method, but are much smoother. A comparison of the two methods is given in Fig. 7.

2. Results

For the $C_{\rm nl}=2000$ simulations, the quasiparticle populations extracted from the simulations are in much better agreement with the energy spectrums from the second-order theory than with those from ordinary Bogoliubov theory. We find that most of the measured distributions for the $C_{\rm nl}=2000$ case are well described by the second-order theory. Sample results are presented in Fig. 8(a).

However, this is not the case for the $C_{\rm nl}=10\,000$ simulations. In fact we find that the energy spectrum is shifted in the opposite direction to that inferred from the simulations,

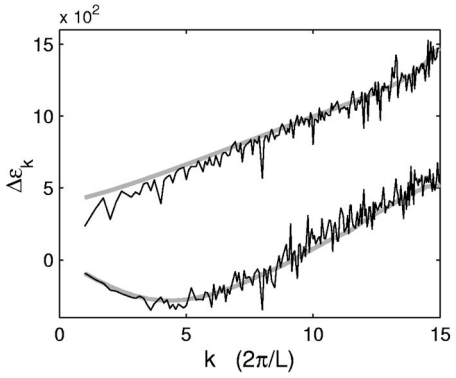

FIG. 7. The shifts to the Bogoliubov quasiparticle energies for two different simulations. The solid thin curves are calculated via the first method described in the text using population data extracted from the simulations, and are hence somewhat noisy. The thick gray curves use the second method, assuming equilibrium populations given by Bogoliubov theory and calculated by numerical integration. The lower curves are for the $C_{\rm nl}=2000$, $\tilde{E}=4000$ simulation, and appear to be approximately gapless as $k\to 0$. The upper curves are for the $C_{\rm nl}=10\,000$, $\tilde{E}=6000$ simulation, and exhibit a gap as $k\to 0$.

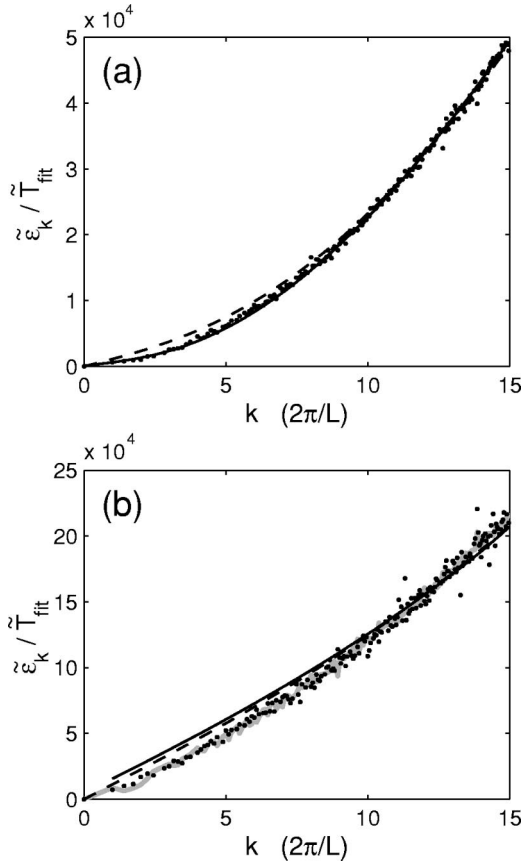

FIG. 8. Fits of the simulation quasiparticle population data to dispersion relations. The dots are a plot of $(N/\langle N_k\rangle - N/\langle N_0\rangle)$, the solid curve is for the dispersion relation predicted by second-order theory, and the dashed curve is the dispersion relation predicted by Bogoliubov theory. (a) $C_{\rm nl}=2000$, $\tilde{E}=4000$, and $\langle N_0\rangle/N=0.279$. Second-order theory gives a good fit to the numerical results with a best-fit temperature of $\tilde{T}=0.201$. (b) $C_{\rm nl}=10\,000$, $\tilde{E}=6000$, and $\langle N_0\rangle/N=0.841$. The shape of the second-order theory dispersion relation does not agree with the population data from the simulation, and the gap is apparent as $k\rightarrow 0$. The gray curve plots the energies as determined by the method described in Sec. VI D with a best-fit temperature of $\tilde{T}=0.0726$.

and that there is an energy gap for $k\rightarrow 0$. The reasons for this are discussed below.

3. Breakdown of perturbation theory

The validity of the second-order theory is constrained by the requirement [5]

$$\left(\frac{k_B T}{n_0 U_0}\right)(n_0 a^3)^{1/2} \ll 1, \tag{38}$$

where n_0 is the condensate density. This corresponds in our dimensionless units to

$$\frac{\tilde{T}}{(8\pi)^{3/2}}\left(\frac{C_{\rm nl}}{\langle N_0\rangle/N}\right)^{1/2} \ll 1. \tag{39}$$

For the results of Fig. 8 with $C_{\rm nl}=2000$, $\tilde{E}=4000$ this parameter is 0.14 and so we are beginning to probe the boundary of validity of the theory. At higher $\tilde{E}$ the shifts become of the order of the unperturbed energies, and hence the results are unreliable. In this region even higher-order terms are important, and the second-order theory can no longer be expected to give good results. From our calculations it seems that this parameter should be $\leqslant 0.2$ for the theory to be valid.

We would like to emphasize, however, that the GPE suffers no such limitations. It is nonperturbative and thus we expect that it will be valid all the way through the transition region, as long as the high-occupation number condition is satisfied.

4. Gaplessness in a finite system

In the course of this work it has become apparent that while the second order theory is gapless for infinite systems, this is not the case for systems such as ours with a finite momentum cutoff. The individual terms in the perturbation expansion given by Eqs. (30) and (32) contain contributions that are proportional to $1/k$ (infrared divergent) and a constant (gap) in the low-k limit. For a homogeneous system these terms cancel exactly when the upper limit of the integrals is infinite, and this leaves a gapless spectrum [5–7]. However, in a system with a momentum cutoff these terms do not exactly cancel, with the result that there is a gap in the predicted excitation spectrum as $k\rightarrow 0$.

Briefly, this gap arises because the energy shifts $\Delta\tilde{E}_4(k)+\Delta\tilde{E}_\lambda(k)$ of Eq. (30) only involve the quantity $\tilde{\kappa}$. This is obtained from Eq. (31) via a sum over all states below the cutoff where the summand depends only on a single wave vector. In contrast the shift $\Delta\tilde{E}_3(k)$ of Eq. (32) involves a sum over states where the summand depends on two wave vectors **i** and **j** (related by momentum conservation) *both* of which must be below the cutoff. This difference in the restrictions on the summations leads to a lack of complete cancellation in the corresponding shifts at low energy and the appearance of a gap in the excitation spectrum.

For the homogeneous gas, we can calculate the size of the gap predicted by the second order theory analytically. Replacing the summations by integrations, we find that the leading order contribution to the energy shift in the limit $k\rightarrow 0$ is

$$\Delta\epsilon_k = \left(\frac{k_B T}{n_0 U_0}\right)(n_0 a^3)^{1/2}\left(\frac{8}{\pi}\right)^{1/2}\frac{\epsilon_k}{y_k(2+y_c^2)} + O(y_k), \tag{40}$$

where $y=k/k_0$ as before and $y_c=k_c/k_0$, where k_c is the momentum cutoff. In the limit $k\rightarrow 0$ we have $\epsilon_k \propto y_k$ and so $\Delta\epsilon_k$ tends to a constant (the gap). The size of the gap tends to zero as the momentum cutoff y_c tends to infinity but otherwise it is finite. We stress that Eq. (40) is only the low-k limit of the exact result. For our simulations there is a minimum wave vector in the problem so it is possible for the terms of order y_k to be larger than the gap contribution given

above. This is the case for the simulations with $C_{\rm nl} \leqslant 2000$, where y_c is reasonably large and the gap is therefore small.

The result of Eq. (40) contains the small parameter that controls the validity of the second-order theory in the usual case where there is no momentum cutoff [cf. Eq. (38)]. However, the result also depends explicitly on the cutoff k_c so in this case there is a second parameter in the theory. For perturbation theory to be valid we require that the predicted energy shifts are small compared to the unperturbed energies, i.e., that $\Delta\epsilon_k/\epsilon_k \ll 1$. We therefore obtain a second criterion for the validity of the second-order theory which is

$$\left(\frac{k_B T}{n_0 U_0}\right)(n_0 a^3)^{1/2}\left(\frac{8}{\pi}\right)^{1/2}\frac{1}{y_k(2+y_c^2)} \ll 1. \tag{41}$$

This result should hold for all momenta in the simulations, and in particular for the smallest value of y_k. For the $C_{\rm nl} = 2000$, $\tilde{E} = 4000$ simulations the left-hand side is 0.04 for $\tilde{k} = 2\pi$. In this case the gap is negligible and the dominant contribution to the energy shifts comes from the terms of order y_k in Eq. (40). The small parameter of the theory is therefore given by Eq. (38). However, for the $C_{\rm nl} = 10\,000$, $\tilde{E} = 5250$ simulations the left-hand side is of order 0.12. In this case the gap is not negligible and we cannot use second-order theory to define a temperature.

This result is somewhat surprising since, even for a condensate fraction of 80% the small parameter of Eq. (38) is of order 0.07, and it does seem reasonable to expect that perturbation theory should be applicable. This does not appear to be the case, however, and we have so far been unable to determine the root cause of this problem. It is worth noting that the numerical simulations themselves have no difficulties in this regime and do not predict a gap at low momentum. This is because the GPE is nonperturbative and indeed this is one of the main reasons for using it to study the properties of Bose condensed systems at finite temperature.

The disagreement between the second-order theory and the numerical simulations is illustrated in Fig. 8(b), where it can be seen that even despite the gap, the shifts the theory predicts are in the wrong direction in comparision with the simulations.

D. Method 3: Nonperturbative determination of the temperature

The failure of second-order theory for the $C_{\rm nl} = 10\,000$ simulations caused us to investigate other possible methods of determining the temperature once the system was in equilibrium. This has led to what seems to be a method of determining the temperature that does not rely on perturbation theory, and we describe it here.

We found earlier that the Bogoliubov spectrum gave a good prediction of the populations of the quasiparticle levels for the lowest energy simulation in the $C_{\rm nl} = 10\,000$ series with $\tilde{E} = 5250$. Therefore, it seems reasonable that the Bogoliubov *basis* should remain a good one for perturbation theory for the next simulation with $\tilde{E} = 5500$, even though the second-order theory cannot be used to calculate the energy shifts.

Therefore, we attempted another method to determine the absolute energy of each quasiparticle level. If we are using a good basis, then on a short-time scale the quasiparticles should be independent, with amplitudes evolving according to

$$b_{\mathbf{k}}(t) = b_{\mathbf{k}}(t_0)\exp[-i\varepsilon_{\mathbf{k}}(t-t_0)/\hbar]. \tag{42}$$

Thus by measuring the gradient of the phase of each quasiparticle we can determine its energy.

To determine the energy spectrum for a single simulation, our numerical procedure was as follows.

(1) Take the last 50 wave functions saved for a simulation once it has reached equilibrium, and evolve each of these individually for a very short period. One hundred wave functions are saved for each of the 50 simulations.

(2) Transform the wave functions into the quasiparticle basis, and measure the energy of each quasiparticle, determined by a linear fit to the phase of each amplitude over all 100 wave functions.

(3) Average over all 50 energy spectrums to give a single three-dimensional spectrum.

(4) Finally, average over angle to give a one-dimensional energy spectrum.

This gives us a dispersion relation $\tilde{\varepsilon}_k - \tilde{\lambda}$ which can then be compared to a plot of $(N/\langle N_k\rangle - N/\langle N_0\rangle)$. If the shapes of the curves agree, then a temperature can be determined via Eq. (26) as in the earlier sections.

We first tested this procedure on the $C_{\rm nl} = 2000$ simulation series, and found that this method was in good agreement with the second-order theory calculations, the two approaches assigning the same temperature to the various simulations.

We then moved onto the $C_{\rm nl} = 10\,000$ simulations. We found the surprising result that not only did the shape of the plots of the curves for $\varepsilon_k/k_B T_{\rm fit}$ and $(1/N_k - 1/N_0)$ agree for the lower-energy simulations where the parameter of Eq. (38) was small, it also agreed when it was of the order of, and greater than one. This was unexpected, as it would seem likely that near the phase transition when interactions are strong that the Bogoliubov quasiparticle basis would no longer be sufficiently good for this method to be accurate. An example of the energy spectrum and its fit to the population data is shown in Fig. 8(b).

As a further test we carried out the same procedure described above, but using the plane-wave basis rather than the Bogoliubov quasiparticle basis. Intuitively it would seem that this would no longer work—but we found that not only did it give the same temperatures as the quasiparticle basis for the $C_{\rm nl} = 10\,000$ simulations, it also agreed with the temperatures determined using second-order theory for the $C_{\rm nl} = 2000$ simulations.

VII. TEMPERATURE DEPENDENCE

Using the three methods described in the preceding section, we have been able to measure an equilibrium tempera-

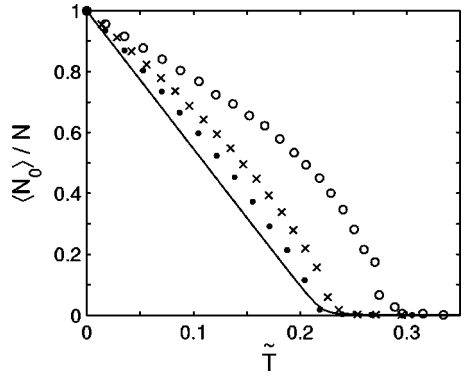

FIG. 9. Condensate fraction versus temperature for the PGPE system with $k<15\times 2\pi/L$ for four different interaction strengths. The open circles are for $C_{\rm nl}=10\,000$, crosses for $C_{\rm nl}=2000$, solid dots for $C_{\rm nl}=500$, and the solid line is for the ideal gas. The shift in the transition temperature is positive with increasing interaction strength $C_{\rm nl}$.

ture for *all* simulations in this paper. We are confident of the results determined from both Bogoliubov and second-order theory; however unfortunately, we do not have any results to compare with for the strongly interacting regime where the nonperturbative method was used. We can only conclude that the temperatures extracted using this method agree numerically with the other two methods in the weakly interacting regime, and that the values obtained seem reasonable and basis independent elsewhere. We intend to test this method further in the future using a numerical ''ideal gas thermometer.''

In this section we move on to consider how other system properties such as condensate fraction, specific heat, and vorticity vary with the temperature $\tilde{T}$.

A. Condensate fraction

It is usual when considering how the condensate fraction varies with the other properties of the system to plot it against temperature, rather than against energy as we have done in Fig. 4. We are now in a position to present this data, and it is displayed in Fig. 9. We can see that a major effect of increasing the nonlinearity is to increase the condensate fraction at any given temperature. This can be understood in the Bogoliubov regime by considering the shape of the dispersion relation.

The Bogoliubov dispersion relation Eq. (28) shows that for a given condensate fraction, a larger value of $C_{\rm nl}$ will result in an increase in the energy of any mode k relative to the condensate. This leads directly to the observation that for a fixed condensate fraction, an increase in the nonlinearity must lead to an increase in the temperature. However, as $\langle N_0\rangle/N\rightarrow 0$ in the transition region, the energy-momentum relationship tends towards the ideal gas dispersion relation, and therefore the transition temperature will not be greatly shifted over a wide range of nonlinearities.

There has been some discussion recently in the literature about the shift in the transition temperature for the homogeneous interacting Bose gas, with some authors even disagreeing on the direction of the shift (e.g., see Ref. [23] and references within). For the PGPE system described in this paper by Eq. (6), we can see from Fig. 9 that the shift is positive, although as yet we have made no effort to quantify this. This would require many more simulations to be run, especially in the transition region, and for the temperatures to be determined more accurately.

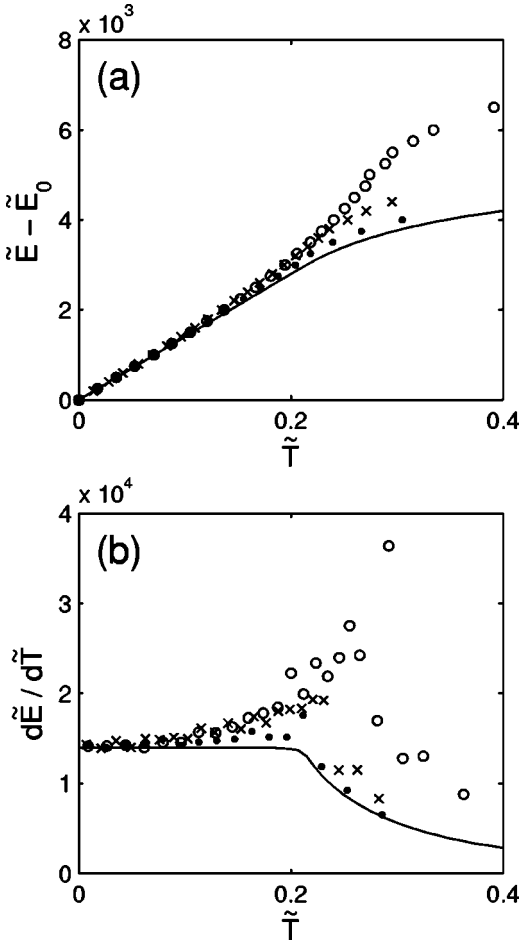

FIG. 10. Graphs relating to the specific heat of the Bose gas in the PGPE model. The open circles are for $C_{\rm nl}=10\,000$, crosses for $C_{\rm nl}=2000$, solid dots for $C_{\rm nl}=500$, and the solid line is for the ideal gas. (a) Plot of the energy versus temperature for all four interaction strengths considered. (b) Plot of the specific heat for all four interaction strengths.

It seems plausible that future simulations of the full FT-GPE (5) or approximations to it could be used to quantitatively measure the shift in the critical temperature for the homogeneous Bose gas when the lowest-energy modes are sufficiently classical. However, the terms coupling the FT-GPE to the effective bath $\hat{\eta}(\mathbf{x})$ may be difficult to implement computationally, and at the present time we are unsure how to proceed in this direction.

B. Specific heat

In Fig. 10(a) we plot the energy of the simulations due to excited states $(\tilde{E}-\tilde{E}_0)$ versus temperature, where $\tilde{E}_0=C_{\rm nl}/2$ is the energy of the system at $\tilde{T}=0$. We can see that

at low temperatures for all interaction strengths this is a straight line, with a slope of about 13 996—the number of excited modes in the system. This is as expected—the average energy contained in a given mode k is

$$\langle \tilde{E}_k \rangle \equiv \frac{\langle N_k \rangle}{N} \tilde{\varepsilon}_k = \frac{\tilde{T}}{\tilde{\varepsilon}_k - \tilde{\mu}} \tilde{\varepsilon}_k \approx \tilde{T}, \tag{43}$$

when there is a condensate present and $\tilde{\mu} \to 0^-$. At higher temperatures, however, the energy rises above the equipartition prediction for nonzero interaction strength $C_{\rm nl}$, and this is an indication that either there are no longer independent modes in the system or more degrees of freedom appear (for example, by the creation of vortices).

The derivative of this curve with respect to temperature gives the specific heat, and this quantity is plotted in Fig. 10(b). The messy nature of this plot is due to small uncertainties in the measured temperature which are amplified when the temperature difference between successive simulations is calculated. However, the plot does display an interesting feature. For nonzero interaction strength, the specific heat appears to reach a peak at the transition temperature, and the height of this peak increases with the value of $C_{\rm nl}$—somewhat reminiscent of the lambda transition in superfluid helium. Once again, further simulations and more accurate determination of the temperature are required for quantitative investigation of this effect. This will be the subject of future work.

C. The role of vortices

A further quantity of interest is the vorticity of the system in equilibrium. It has been argued that vortices may be important in the superfluid transition of ^{4}He, reducing the superfluid density near the transition point [24]. With this in mind, we have studied the presence of vortex lines in our simulations. Recently Berloff and Svistunov [25] have considered the evolution of topological defects in the evolution of a Bose gas from a strongly nonequilibrium state.

A vortex is a topological excitation, characterized in a wave function by

$$\oint_C \nabla \, \mathrm{Arg}[\psi(\mathbf{x})] \cdot d\mathbf{l} = 2\pi n, \tag{44}$$

where C is a closed contour, and n is a nonzero integer, the sign of which indicates the circulation of the vortex. The continuous variation of the phase from zero to $2n\pi$ around such a contour implies that there must be a discontinuity in the phase within the loop. The only way that this can be physical is for the wave function to have zero amplitude at the spatial position of the phase singularity.

In a two-dimensional wave function the center of vortices are zero-dimensional points, and they can be easily counted to give a measure of the vorticity of the system. However, in three dimensions vortices form lines and rings, and the equivalent quantity of the 2D measure of vorticity would be to calculate the length of all vortex structures in the wave function. This would be a somewhat complicated procedure numerically, and so we have devised a different technique.

We increase the spatial resolution of our wave functions to be $128 \times 128 \times 128$ points, so that the grid spacing is smaller than the vortex healing length ξ, defined by

$$\frac{\hbar^2}{2m\xi^2} = n_0 U_0 . \tag{45}$$

We do this by extending the wave function in k space, and then Fourier transforming to real space. This does not require any extra information, as for $k > 15 \times 2\pi/L$ we have $c_{\mathbf{k}} = 0$. We then count the number of vortex lines passing through every xy plane, and take the average over all planes. It seems that this is a reasonable measure of the vorticity of the wave function, and it should be similar to the measurement of the length of the vortex structures discussed above.

We have analyzed the data from the simulations using this procedure. We find that when the energy of the simulation is sufficiently high that there are vortices present, the time evolution of the vorticity is a good indicator for when the system reaches equilibrium. As is the case for the condensate population, the vorticity tends to an equilibrium value which fluctuates by a small amount (much smaller than the fluctuations in the condensate population).

A plot of the vorticity against system energy is shown in Fig. 11(a) for the $C_{\rm nl} = 10\,000$ simulation (the curves are qualitatively similar for the other nonlinearities). We see that there is a minimum energy required for vortices to be present in the system at equilibrium. Also, as we reach this energy the plot of condensate occupation versus energy appears to dip. This same behavior is observed for the $C_{\rm nl} = 500$ and 2000 cases, but it occurs at a higher condensate fraction, and is not as pronounced. There is no corresponding departure from linearity in the ideal gas case, as was seen in Fig. 4(b).

A plot of the number of vortex lines versus temperature for all the simulations is shown in Fig. 11(b), and this displays a large increase in the vorticity near the transition temperature for $C_{\rm nl} = 10\,000$. A more in-depth analysis of this behavior will be carried out in a subsequent extension of this work.

Finally, a three-dimensional visualization of the network of vortex lines is shown in Fig. 12 for three simulation energies for the $C_{\rm nl} = 10\,000$ simulations. Each point corresponds to where a vortex line was detected in the horizontal planes, and for the lowest two energies several vortex rings are clearly visible.

VIII. CONCLUSIONS

We have presented what we believe is compelling evidence that the projected Gross-Pitaevskii equation is a good approximation to the dynamics of the classical modes of a Bose gas. We have described how to carry out the projection technique in the homogeneous case with periodic boundary conditions, and have shown that starting with a randomized wave function with a given energy, the projected GPE evolves towards an equilibrium state. We have analyzed the numerical data in terms of quadratic Bogoliubov theory, and also the gapless, finite temperature theory of Ref. [5] in the

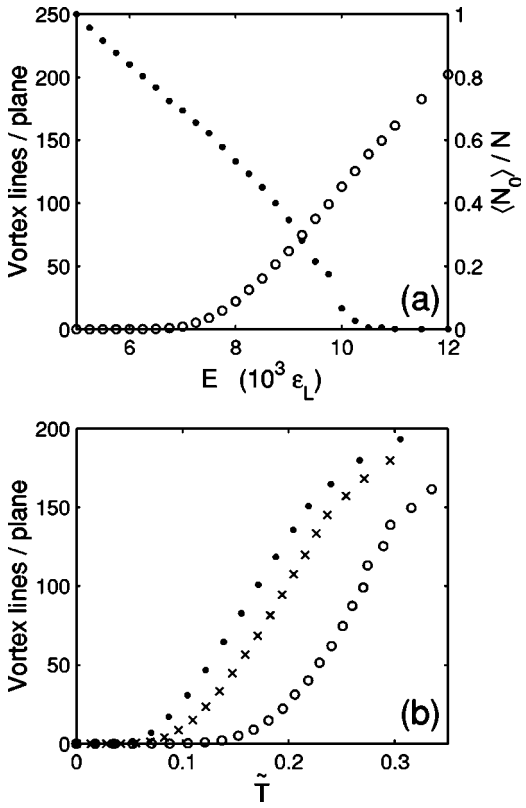

FIG. 11. The presence of vortices in the simulations. (a) A plot of vorticity for the $C_{\rm nl}=10\,000$ simulation series. The number of vortex lines per plane are indicated by open circles with the scale on the left vertical axis, and the condensate fraction by dots with the scale on the right vertical axis. (b) The number of vortex lines per plane plotted against temperature for all three simulation series. Open circles are $C_{\rm nl}=10\,000$, crosses are $C_{\rm nl}=2000$, and dots are $C_{\rm nl}=500$.

classical limit. We have found that both the occupation and energies of the quasiparticles agree quantitatively with the predictions when these theories are valid.

Outside the range of perturbation theory we have proposed another technique that has allowed us to determine a temperature for the PGPE simulations in equilibrium. This method agrees with the perturbative methods when they are valid. Using this definition, we have found that increasing the nonlinearity $C_{\rm nl}$ leads to an increase in both the transition temperature and the specific heat of the system at the critical point. We have also presented evidence that suggests vortices may play some role in the transition. The projected GPE is a simple equation but it appears to describe very rich physics, only some of which we have considered here.

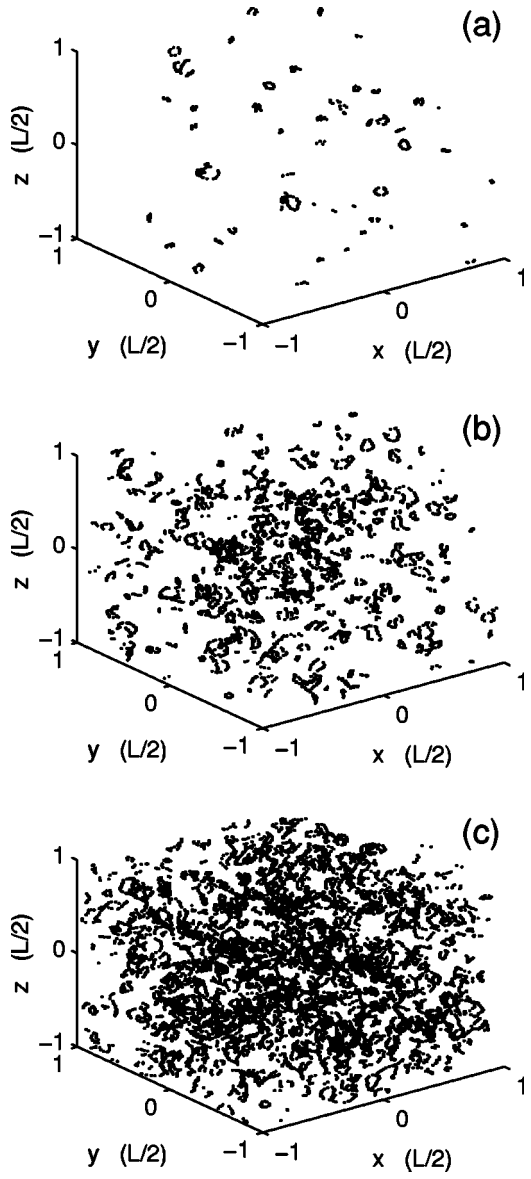

FIG. 12. A visualization of the vortex network in equilibrium for the case of $C_{\rm nl}=10\,000$. (a) $\tilde{E}=7000$, (b) $\tilde{E}=8000$, (c) $\tilde{E}=9000$. Each point corresponds to where a vortex line was detected in the horizontal plane. Several vortex rings are visible in the figures.

ACKNOWLEDGMENTS

The authors would like to thank R. J. Ballagh and C. W. Gardiner for useful discussions. This work was financially supported by St. John's College and Trinity College, Oxford, and the UK-EPSRC.

[1] M. J. Davis, R. J. Ballagh, and K. Burnett, J. Phys. B **34**, 4487 (2001).
[2] M. Anderson, J. R. Ensher, M. R. Matthews, C. E. Wieman, and E. A. Cornell, Science **269**, 198 (1995).
[3] K. B. Davis, M.-O. Mewes, M. R. Andrews, N. J. van Druten, D. S. Durfee, D. M. Kurn, and W. Ketterle, Phys. Rev. Lett. **75**, 3969 (1995).
[4] C. C. Bradley, C. A. Sackett, J. J. Tollet, and R. G. Hulet, Phys. Rev. Lett. **75**, 1687 (1995).
[5] S. A. Morgan, J. Phys. B **33**, 3847 (2000).

[6] P. O. Fedichev and G. V. Shlyapnikov, Phys. Rev. A **58**, 3146 (1998).
[7] S. Giorgini, Phys. Rev. A **61**, 063615 (2000).
[8] M. J. Davis, S. A. Morgan, and K. Burnett, Phys. Rev. Lett. **87**, 160402 (2001).
[9] B. V. Svistunov, J. Mosc. Phys. Soc. **1**, 373 (1991).
[10] Yu. Kagan, B. V. Svistunov, and G. V. Shlyapnikov, Zh. Éksp. Teor. Fiz. **101**, 528 (1992) [Sov. Phys. JETP **75**, 387 (1992)].
[11] Yu. Kagan and B. V. Svistunov, Zh. Éksp. Teor. Fiz. **105**, 353 (1994) [Sov. Phys. JETP **78**, 187 (1994)].
[12] Yu. Kagan and B. V. Svistunov, Phys. Rev. Lett. **79**, 3331 (1997).
[13] K. Damle, S. N. Majumdar, and S. Sachdev, Phys. Rev. A **54**, 5037 (1996).
[14] R. J. Marshall, G. H. C. New, K. Burnett, and S. Choi, Phys. Rev. A **59**, 2085 (1999).
[15] A. Sinatra, Y. Castin, and C. Lobo, J. Mod. Opt. **47**, 2629 (2000).
[16] A. Sinatra, C. Lobo, and Y. Castin, Phys. Rev. Lett. **87**, 210404 (2001).
[17] A. Sinatra, C. Lobo, and Y. Castin, e-print cond-mat/0203259.
[18] K. Gòral, M. Gajda, and K. Rzążewski, Opt. Express **8**, 92 (2001).
[19] K. Góral, M. Gajda, and K. Rzążewski, e-print cond-mat/0203259.
[20] H. T. C. Stoof and M. J. Bijlsma, J. Low Temp. Phys. **124**, 431 (2001).
[21] G. D. Moore and N. Turok, Phys. Rev. D **55**, 6538 (1997).
[22] L. E. Reichl, *A Modern Course in Statistical Physics* (University of Texas Press, Austin, 1980).
[23] P. Arnold, G. Moore, and B. Tomášik, Phys. Rev. A **65**, 013606 (2002).
[24] G. A. Williams, J. Low Temp. Phys. **89**, 91 (1992).
[25] N. G. Berloff and B. V. Svistunov, Phys. Rev. A **66**, 013603 (2002).